Shock-Tube Studies on the Reactions of $CF_2(X^1A_1)$ with $O(^3P)$ and H Atoms

Yasuyuki Yamamori, Kazuo Takahashi,* and Tadaaki Inomata

Department of Chemistry, Sophia University, 7-1 Kioi-cho, Chiyoda-ku, Tokyo 102-8554, Japan

Received: May 19, 1999; In Final Form: August 6, 1999

The reactions of $CF_2(X^1A_1)$ radicals with $O(^3P)$ and H atoms have been studied by using a shock tube/atomic resonance absorption spectroscopy technique over the temperature ranges 2000−2430 and 1450−1860 K and the total density range 6.1×10^{18} to 1.2×10^{19} molecules cm^{-3}. Nitrous oxide and ethyl iodide were used as precursors of $O(^3P)$ and H atoms, respectively. Electronically ground state $CF_2(X^1A_1)$ radicals were produced through the thermal decomposition of chlorodifluoromethane. The rate coefficients for the reactions $CF_2(X^1A_1) + O(^3P)$ and $CF_2(X^1A_1) + H$ were obtained from the decay profiles of O and H atom concentrations as $k(CF_2+O) = 10^{-10.39\pm0.07}$ and $k(CF_2+H) = 10^{-10.18\pm0.21} \exp[-(19.0 \pm 6.7)\ \text{kJ mol}^{-1}/RT]\ \text{cm}^3\ \text{molecule}^{-1}\ \text{s}^{-1}$ (error limits at the two standard deviation level). Neither rate coefficient had any pressure dependence under the present experimental conditions. The G2-level ab initio molecular orbital calculation was also performed to examine the product channels for the $CF_2(X^1A_1) + O(^3P)$ and $CF_2(X^1A_1) + H$ reactions. The theoretical calculation showed that the most energetically favorable pathways for $CF_2(X^1A_1) + O(^3P)$ and $CF_2(X^1A_1) + H$ systems were the channels producing FCO + F and CF + HF, respectively. The G2 energy of the transition state for the channel $CF_2(X^1A_1) + O(^3P) \rightarrow$ FCO + F was 116 kJ mol^{-1} lower than that of the reactants $CF_2(X^1A_1) + O(^3P)$, while the energy of the three-centered transition state for the channel $CF_2(X^1A_1) + H \rightarrow$ CF + HF is 45 kJ mol^{-1} higher than that of the reactants $CF_2(X^1A_1) + H$. These results could qualitatively explain the difference of the temperature dependence observed between $k(CF_2+O)$ and $k(CF_2+H)$.

Introduction

Halons, bromine-containing perhalogenated carbon compounds such as CF_3Br, CF_2BrCl, and $C_2F_4Br_2$, have been used for many years as gaseous fire-extinguishing agents. They have high fire-extinguishing abilities because of their chemical suppression mechanism, that is, bromine-containing species can catalytically remove active species from the combustion zone. Because of serious concerns about ozone depletion in the stratospheric, however, the production of halons has already been prohibited and intensive research has been undertaken to find effective replacements. A few years ago, trifluoromethane (CHF_3, HFC-23) was proposed as one of the candidates to replace halons. Although HFC-23 has already begun to be produced as a commercial fire-extinguishing agent, its flame-suppression mechanism is not known yet.

Some groups[1,2] have already constructed the reaction mechanisms for hydrofluorocarbons (HFCs) to understand the chemical role of HFC-23 in a flame and/or to find other HFCs that have higher fire-extinguishing abilities. In particular, a detailed chemical kinetic model for C1- and C2-hydrofluorocarbons published by the NIST group,[1] which consists of 55 species and 589 elementary reactions, is widely applied to the numerical simulation for HFC-inhibited flames. Nevertheless, this reaction mechanism is not clear enough to examine experimental results comprehensively, because the kinetic data for a large number of elementary reactions included in the mechanism have not directly been measured at high temperatures.

To solve this problem, we have performed kinetic studies on some important reactions for the HFC-23 combustion by using a shock tube; we reported rate coefficients for the reactions $CHF_3 + H \rightarrow CF_3 + H_2$, $CF_3 + H \rightarrow CF_2(X^1A_1) + HF$, and $CF_3 + O(^3P) \rightarrow F_2CO(X^1A_1) + F$ in our earlier papers.[3,4] These kinetic studies also showed that $CF_2(X^1A_1)$ and $F_2CO(X^1A_1)$ were major intermediates produced in the CHF_3 combustion. So, as the next part of our research on the flame suppression by CHF_3, we focus on the high-temperature kinetics of the subsequent reactions of $CF_2(X^1A_1)$ radicals with some active species in the combustion.

$$CF_2(X^1A_1) + O(^3P) \rightarrow \text{products} \quad (1)$$

$$CF_2(X^1A_1) + H \rightarrow \text{products} \quad (2)$$

Reactions 1 and 2 also have practical significance in the fields of plasma chemistry and atmospheric chemistry, and several kinetic studies on these reactions have been reported at room temperature. The overall rate coefficient for reaction 1 was first determined by Ryan and Plumb[5] using a discharge flow/mass spectroscopy technique to be $k(CF_2+O) = (1.8 \pm 0.4) \times 10^{-11}$ cm^3 $molecule^{-1}$ s^{-1}. Subsequently, Tsai and McFadden[6] obtained $k(CF_2+O) = (2.0 \pm 0.4) \times 10^{-11}$ cm^3 $molecule^{-1}$ s^{-1} by the discharge flow experiments with a photoionization mass spectrometer, in good agreement with the result of Ryan and Plumb. Two other studies,[7,8] which were performed by using laser-induced fluorescence, also reported almost the same values as $k(CF_2+O)$. On the contrary, there is a great difference in the rate coefficient for reaction 2 between two previous room-temperature studies; $k(CF_2+H) = (1.7 \pm 0.4) \times 10^{-13}$ cm^3 $molecule^{-1}$ s^{-1} reported by Ryan and Plumb[9] and $k(CF_2+H) = (3.9 \pm 0.7) \times 10^{-11}$ cm^3 $molecule^{-1}$ s^{-1} by Tsai and McFadden,[10] indicating that the $k(CF_2+H)$ values are still unsettled even at room temperature.

On the other hand, the high-temperature experimental results were previously published only by Biordi et al.[11] to be

* Corresponding author.Phone: +81-3-3238-3457. Fax: +81-3-3238-3478. E-mail: takaha-k@hoffman.cc.sophia.ac.jp.

10.1021/jp991652g CCC: $18.00
Published on Web 10/14/1999

TABLE 1: Experimental Conditions

reaction	composition of test gas mixture/ppm $CHClF_2$	N_2O	C_2H_5I	monitored atom	temperature/ K	total density/ molecules cm^{-3}
$CF_2(X^1A_1) + O(^3P)$	16−32	8−16		$O(^3P)$	2000−2430	6.1×10^{18} to 1.2×10^{19}
$CF_2(X^1A_1) + H$	8−16		1−2	H	1450−1860	6.1×10^{18} to 1.2×10^{19}

$k(CF_2+O) = 8.30 \times 10^{-11}$ and $k(CF_3+H) = 3.32 \times 10^{-11}$ cm^3 $molecule^{-1}$ s^{-1} (1800 K). However, there is some possibility that the data of Biordi et al. were influenced by secondary reactions, because they were determined in methane−oxygen−argon flames containing CF_3Br where complicated branching reactions occur simultaneously. These rate coefficients published in the NIST kinetic model[1] are simply estimated values which were made by giving small activation barriers (4−5 kJ mol^{-1}) to the room-temperature data of Tsai and McFadden.[6,10] Therefore, more accurate kinetic data for reactions 1 and 2 are needed to construct a better reaction mechanism for the hydrofluorocarbons at high temperatures.

In the present study, the rate coefficients for reactions 1 and 2 were experimentally determined by using a shock tube/atomic resonance absorption spectroscopy technique over the temperature ranges of 2000−2430 and 1450−1860 K, respectively. An ab initio molecular orbital calculation was also performed to examine the product channels of these reactions.

Experimental Section

Shock Tube and Optical System. All experiments were performed behind reflected shock waves in a diaphragmless stainless steel shock tube, which consists of a 5.84 *l* driver section and a 6.2 cm i.d. and 4.6 m long test section. The details of its structure and its performance have been described previously.[3] The test section was evacuated by a turbomolecular pump to pressures down to 1×10^{-6} Torr, in which the residual gas was practically free from hydrocarbons. To measure incident shock velocity, three piezoelectric pressure transducers were mounted on the shock tube walls at 25 cm intervals from the end of the test section. Temperature and pressure of the shock-heated test gas were calculated from the incident shock velocity using standard methods.

The time-resolved concentrations of electronically ground state $O(^3P_J)$ and $H(^2S_{1/2})$ atoms were monitored by atomic resonance absorption spectroscopy (ARAS). A microwave discharge lamp, in which helium containing a few percent of oxygen or hydrogen was flowing at a pressure of 4 Torr, was used as a light source of O- or H-ARAS. The wavelengths of monitored resonance light were 130.2, 130.4, and 130.6 nm ($^3S_1 \leftarrow {}^3P_J$) for O atoms and 121.6 nm ($^2P_J \leftarrow {}^2S_{1/2}$) for H atoms. The resonant radiation from the lamp passed through two MgF_2 windows (1 mm thickness) mounted on the shock tube walls at a position 2 cm from the end plate. The transmitted light was isolated by a 20 cm VUV monochromator (Minutesman 302-VM), which was evacuated to a pressure less than 4×10^{-5} Torr and detected by a solar-blind photomultiplier tube (Hamamatsu Photonics R1459). The signal was then recorded by a digital storage oscilloscope (Hitachi VC-6165).

Measurements and Gases. Measurements of the rate coefficient for the $CF_2(X^1A_1) + O(^3P)$ reaction were carried out in mixtures of $CHClF_2-N_2O-Ar$ by detecting O atoms, while the rate coefficient for the $CF_2(X^1A_1) + H$ was obtained from the decay of H atoms in mixtures of $CHClF_2-C_2H_5I-Ar$. The details of these experimental conditions are shown in Table 1. Under the present experimental conditions, electronically ground state $CF_2(X^1A_1)$ radicals are rapidly produced through the thermal decomposition of $CHClF_2$. Triplet electronic state oxygen atoms are formed through the thermal decomposition of N_2O, although the production rate of $O(^3P)$ atoms is much slower than that of $CF_2(X^1A_1)$ radicals. Hydrogen atoms are instantaneously formed through the thermal decomposition of C_2H_5I. Oxygen and hydrogen atoms might also be generated due to wall contaminations or resident impurities so that blank tests with argon alone were performed during the measurements, confirming the absence of background signals. The calibration experiments for O-ARAS were performed in 1−20 ppm of N_2O-Ar mixtures at temperatures of approximately 2000 and 3000 K, while those for H-ARAS were done in 0.5−2 ppm of C_2H_5I-Ar mixtures at temperatures of 1450, 1650, and 1850 K. These calibration results have been described elsewhere.[3,4]

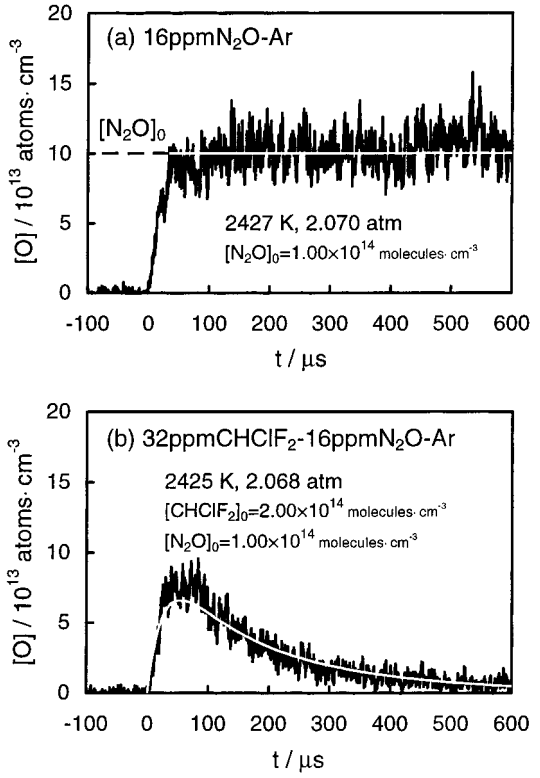

Figure 1. Typical concentration profiles of (a) O atoms in 16 ppm of N_2O-Ar, (b) O atoms in 32 ppm of $CHClF_2-16$ ppm of N_2O-Ar mixtures. The white curve in part b denotes the profile calculated in the reaction scheme of Table 2.

High purity helium (99.995%) was used as the driver gas. Scientific grade argon (99.9999%) was used as the diluent gas. Ethyl iodide was purified by trap-to-trap distillation. Chlorodifluoromethane (99.7%) and research grade nitrous oxide (99.99%) were used without further purification.

Experimental Results

$CF_2(X^1A_1) + O(^3P)$ Reaction. Measurements of the rate coefficient for the $CF_2(X^1A_1) + O(^3P)$ reaction were carried out in mixtures of $CHClF_2$ and N_2O highly diluted in argon. Figure 1 shows typical concentration profiles of O atoms in 16 ppm of N_2O-Ar mixtures (a) without $CHClF_2$ and (b) with 32

TABLE 2: Reaction Scheme for the $CHClF_2-N_2O$ System

		forward rate coefficient[a]			
no.	reaction	log A	n	E_a/R	ref
(1)	$CF_2(X^1A_1) + O = FCO + F$	adjusted			
(3)	$N_2O + M = N_2 + O + M$	−9.57	0.00	26 000	13
(4)	$CHClF_2 + M = CF_2(X^1A_1) + HCl + M$	−8.62	0.00	20 200	12
(5)	$FCO + M = F + CO + M$	−9.62	0.00	15 100	14
(6)	$FCO + O = CO + FO$	−9.78	0.00	0	14
(7)	$CF_2(X^1A_1) + CF_2(X^1A_1) = C_2F_4$	−13.14	0.50	200	15
(8)	$O + O + M = O_2 + M$	−34.28	0.00	−900	16

[a] Forward rate coefficients in the form $k = AT^n \exp(-E_a/RT)$, in cm^3, molecule, and s units. Reverse rate coefficients were calculated from the forward ones and the equilibrium constants.

ppm of $CHClF_2$. Time zero in the figure denotes the arrival of a reflected shock wave at the optical pathway. In the N_2O-Ar mixture, the O atom concentration increases gradually through reaction 3 to reach a nearly constant value, which is corresponding to the initial concentration of N_2O, as shown with the white line in Figure 1a.

$$N_2O + M \rightarrow N_2 + O(^3P) + M \qquad (3)$$

In the presence of $CHClF_2$, oxygen atoms get to a maximum value at 70 μs and then decay. As reported by Su et al.,[12] $CHClF_2$ is decomposed through the following three-centered elimination reaction:

$$CHClF_2 + M \rightarrow CF_2(X^1A_1) + HCl + M \qquad (4)$$

Under the present experimental conditions, the rate of reaction 4 is sufficiently faster than that of reaction 3. From the kinetic data for reaction 4,[12] the times when 99% of $CHClF_2$ is decomposed to $CF_2(X^1A_1)$ and HCl are calculated to be 4.67 μs at 2000 K and 0.78 μs at 2430 K with a total density of 1.0×10^{19} molecules cm^{-3}. Therefore, the O atom decay after 70 μs found in Figure 1b is caused by the $CF_2(X^1A_1) + O(^3P)$ reaction, but not by the $CHClF_2 + O(^3P)$ reaction.

To determine the rate coefficient for reaction 1, the concentration profiles of O atoms were calculated by numerically integrating the rate equations in the appropriate reaction scheme of Table 2. In the numerical calculation, the products of reaction 1 were treated as FCO and F, because the ab initio MO calculation could specify these products, as discussed later. Although we also tried to determine k_1 assuming other products such as CF + FO and CO + F_2, the values of k_1 were not changed in the least, because the subsequent reactions of FCO, F, CF, FO, CO, and F_2 with $O(^3P)$ atoms were negligible under the present experimental conditions and had no sensitivities to O atom concentration. The value of k_1 was adjusted so that the calculated curve most closely matched the observed one, as shown with the white line in Figure 1b. Rate coefficient data for reaction 1, derived under various experimental conditions, are summarized in Table 3. The Arrhenius plot of k_1 is shown in Figure 2, together with the previous data estimated by the

TABLE 3: Summary of Rate Coefficients Measured for the Reaction $CF_2(X^1A_1) + O(^3P) \rightarrow FCO + F$

		reflected shock region				
P_1[a] Torr	U_s[b] m ms^{-1}	T K	[M] molecules cm^{-3}	$[CHClF_2]_0$ molecules cm^{-3}	$[N_2O]_0$ molecules cm^{-3}	k_1 cm^3 molecule^{-1} s^{-1}
			[M] = 6.1×10^{18} molecules cm^{-3}			
30.0	0.932	2017	6.24×10^{18}	2.00×10^{14}	9.99×10^{13}	3.65×10^{-11}
30.0	0.946	2074	6.32×10^{18}	2.02×10^{14}	1.01×10^{14}	3.32×10^{-11}
29.0	0.948	2082	6.12×10^{18}	1.96×10^{14}	9.79×10^{13}	3.99×10^{-11}
29.0	0.966	2158	6.21×10^{18}	1.99×10^{14}	9.93×10^{13}	4.15×10^{-11}
29.0	0.975	2198	6.25×10^{18}	2.00×10^{14}	1.00×10^{14}	4.32×10^{-11}
29.0	0.985	2239	6.29×10^{18}	2.01×10^{14}	1.01×10^{14}	4.32×10^{-11}
29.0	0.988	2251	6.31×10^{18}	2.02×10^{14}	1.01×10^{14}	4.32×10^{-11}
29.0	0.998	2295	6.35×10^{18}	2.03×10^{14}	1.02×10^{14}	4.15×10^{-11}
28.0	1.011	2352	6.19×10^{18}	1.98×10^{14}	9.91×10^{13}	4.32×10^{-11}
28.0	1.021	2395	6.23×10^{18}	1.99×10^{14}	9.97×10^{13}	4.48×10^{-11}
28.0	1.023	2404	6.24×10^{18}	2.00×10^{14}	9.98×10^{13}	4.15×10^{-11}
28.0	1.025	2415	6.25×10^{18}	2.00×10^{14}	1.00×10^{14}	3.82×10^{-11}
28.0	1.028	2425	6.26×10^{18}	2.00×10^{14}	1.00×10^{14}	4.15×10^{-11}
			[M] = 1.2×10^{19} molecules cm^{-3}			
60.0	0.954	2019	1.25×10^{19}	2.00×10^{14}	1.00×10^{14}	4.65×10^{-11}
60.0	0.934	2027	1.25×10^{19}	2.00×10^{14}	1.00×10^{14}	4.32×10^{-11}
59.0	0.942	2059	1.24×10^{19}	1.98×10^{14}	9.91×10^{13}	4.48×10^{-11}
59.0	0.945	2069	1.24×10^{19}	1.99×10^{14}	9.93×10^{13}	3.49×10^{-11}
57.0	0.953	2105	1.21×10^{19}	1.93×10^{14}	9.66×10^{13}	3.82×10^{-11}
52.0	0.954	2108	1.10×10^{19}	1.76×10^{14}	8.82×10^{13}	4.15×10^{-11}
58.0	0.961	2138	1.24×10^{19}	1.98×10^{14}	9.89×10^{13}	4.15×10^{-11}
56.0	0.967	2163	1.20×10^{19}	1.92×10^{14}	9.59×10^{13}	4.48×10^{-11}
57.0	0.968	2168	1.22×10^{19}	1.95×10^{14}	9.77×10^{13}	4.15×10^{-11}
57.0	0.970	2176	1.22×10^{19}	1.96×10^{14}	9.79×10^{13}	4.15×10^{-11}
57.0	0.977	2203	1.23×10^{19}	1.97×10^{14}	9.83×10^{13}	3.82×10^{-11}
56.0	0.984	2236	1.21×10^{19}	1.94×10^{14}	9.72×10^{13}	4.15×10^{-11}
56.0	0.987	2247	1.22×10^{19}	1.95×10^{14}	9.74×10^{13}	4.15×10^{-11}
56.0	0.990	2259	1.22×10^{19}	1.95×10^{14}	9.76×10^{13}	4.65×10^{-11}
56.0	0.997	2290	1.23×10^{19}	1.96×10^{14}	9.80×10^{13}	3.99×10^{-11}
56.0	1.006	2328	1.23×10^{19}	1.97×10^{14}	9.87×10^{13}	4.32×10^{-11}
56.0	1.008	2339	1.24×10^{19}	1.98×10^{14}	9.88×10^{13}	4.15×10^{-11}
56.0	1.009	2342	1.24×10^{19}	1.98×10^{14}	9.89×10^{13}	4.48×10^{-11}
55.0	1.014	2364	1.22×10^{19}	1.95×10^{14}	9.74×10^{13}	3.99×10^{-11}
55.0	1.028	2429	1.23×10^{19}	1.97×10^{14}	9.87×10^{13}	3.82×10^{-11}

[a] Pressure ahead of incident shock wave. [b] Incident shock velocity.

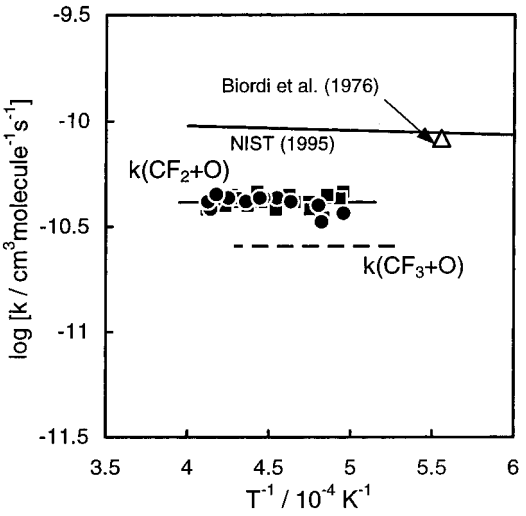

Figure 2. Arrhenius plot of the rate coefficients for the $CF_2(X^1A_1)$ + $O(^3P)$ reaction. (●) and (■) denote the present results measured at $[M] = 6.2 \times 10^{18}$ and 1.2×10^{19} molecules cm^{-3}, respectively. (△) denotes the previous value reported by Biordi et al.[11] Solid line (—) denotes the recommended data by the NIST group.[1] (- - -) denotes the rate coefficient for the $CF_3 + O(^3P)$ reaction determined by our group.[4]

NIST group[1] and reported by Biordi et al.[11] Our rate coefficient has neither temperature nor pressure dependence. Over the temperature range of 2000−2430 K, the average value of k_1 was obtained as follows:

$$k_1 = 10^{-10.39\pm0.07}\ \text{cm}^3\ \text{molecule}^{-1}\ \text{s}^{-1}$$

where the error limit means two standard deviations.

$CF_2(X^1A_1)$ + H Reaction. To determine the rate coefficient for the $CF_2(X^1A_1)$ + H reaction, the decay profiles of H atom concentration were measured in mixtures of $CHClF_2$ and C_2H_5I highly diluted in argon. Figure 3 shows typical concentration profiles of H atoms in 1 ppm of C_2H_5I−Ar mixtures (a) without $CHClF_2$ and (b) with 8 ppm of $CHClF_2$. In the C_2H_5I−Ar mixture, the H atom concentration instantaneously rises to reach a nearly constant value. At the present experimental temperatures, ethyl iodide is decomposed through the following competing channels:

$$C_2H_5I \rightarrow C_2H_5 + I \quad (9a)$$

$$C_2H_5I \rightarrow C_2H_4 + HI \quad (9b)$$

The ethyl radicals produced through reaction 9a immediately decay to become ethylene and hydrogen atoms.

$$C_2H_5(+M) \rightarrow C_2H_4 + H(+M) \quad (-10)$$

If other reactions producing and consuming hydrogen atoms do not occur along with the above reactions, the final H atom concentration $[H]_f$ can be related to the initial concentration of ethyl iodide by the following formula:

$$[H]_f = \frac{k_{9a}}{k_{9a} + k_{9b}}[C_2H_5I]_0$$

As shown in Figure 3a, $[H]_f$ calculated from this expression is in good agreement with the final value of H atom concentration obtained experimentally. This confirms that the formation of hydrogen atom from ethyl iodide can be explained only by

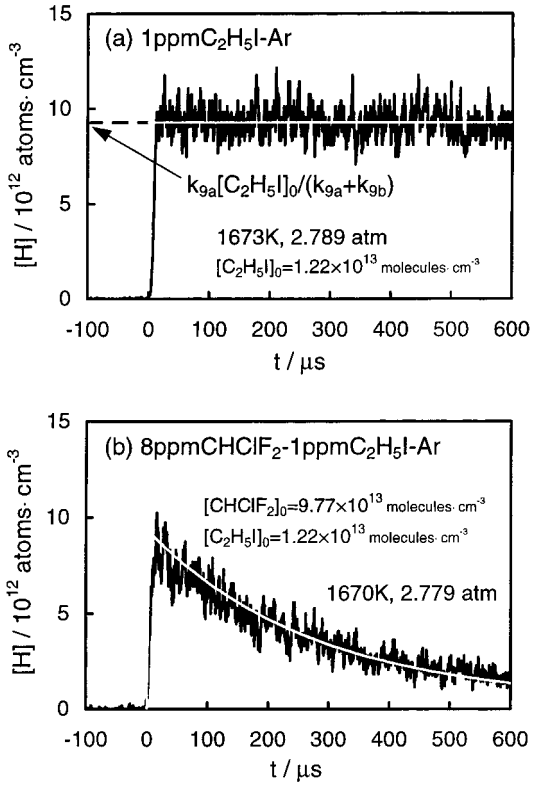

Figure 3. Typical concentration profiles of (a) H atoms in 1 ppm of C_2H_5I−Ar, (b) H atoms in 8 ppm of $CHClF_2$−1 ppm of C_2H_5I−Ar mixtures. The white curve in part b denotes the profile calculated in the reaction scheme of Table 4.

reactions 9a, 9b, and −10. On the other hand, in the $CHClF_2$−C_2H_5I−Ar mixture, H atoms were gradually reduced after the initial production. As mentioned above, $CHClF_2$ is easily decomposed to $CF_2(X^1A_1)$ and HCl at temperatures above 1400 K. The rate of the $CHClF_2$ thermal decomposition is much faster than the rate of the reaction $CHClF_2$ + H under the present experimental conditions. High-temperature kinetic data for the reaction $CHClF_2$ + H have been published by Richter et al.[17] The branching ratios, $k_4[M]/\{k_4[M] + k(CHClF_2+H)[H]_f\}$, are calculated to be 0.997 at 1450 K and 0.999 at 1860 K with $[M] = 1.0 \times 10^{19}$ and $[H]_f = 2.0 \times 10^{13}$ molecules cm^{-3}, indicating that almost all $CHClF_2$ molecules are decomposed to $CF_2(X^1A_1)$ + HCl before reacting with H atoms. This confirms that the H atom decay found in Figure 3b is caused by the reaction with $CF_2(X^1A_1)$ but not with $CHClF_2$.

The rate coefficient for reaction 2 was optimized by fitting calculated H atom concentrations to observed ones, in the same way as the determination of k_1. The reaction scheme used for the numerical calculation is listed in Table 4. In this scheme, the products of reaction 2 were defined as CF and HF, based on the results of the ab initio MO calculation, as discussed later. However, the choice of products was preliminarily checked to give no serious error for the determination of k_2 under the present experimental conditions. Optimization results of k_2, derived under various experimental conditions, are summarized in Table 5; the Arrhenius plot is shown in Figure 4, with the previous data estimated by the NIST group[1] and reported by Biordi et al.[11] The rate coefficient measured in the present work has a slight positive temperature dependence, although reaction 2 is one of atom−radical reactions which normally have little or no temperature dependence. A linear least-squares fit of the experimental data yielded the following Arrhenius expression over the temperature range 1450−1860 K:

TABLE 4: Reaction Scheme for the $CHClF_2-C_2H_5I$ System

			forward rate coefficient[a]			
no.	reaction		log A	n	E_a/R	ref
(2)	$CF_2(X^1A_1) + H = CF + HF$			adjusted		
(4)	$CHClF_2 + M = CF_2(X^1A_1) + HCl + M$		−8.62	0.00	20200	12
(7)	$CF_2(X^1A_1) + CF_2(X^1A_1) = C_2F_4$		−13.14	0.50	200	15
(9a)	$C_2H_5I = C_2H_5 + I$		11.79	0.00	20200	18
(9b)	$C_2H_5I = C_2H_4 + HI$		11.11	0.00	19500	18
(10)	$H + C_2H_4(+M) = C_2H_5(+M)$	high	−10.44	0.00	1030	13
		low	−19.76	−2.80	−24	13
(11)	$C_2H_5I + H = C_2H_5 + HI$		−9.24	0.00	1760	19
(12)	$C_2H_5I + I = C_2H_5 + I_2$		−10.18	0.00	8410	19
(13)	$F + F + M = F_2 + M$		−33.56	0.00	0	19
(14)	$F + H + M = HF + M$		−29.58	−1.00	0	19
(15)	$F_2 + H = HF + F$		−9.70	0.00	1210	19
(16)	$HF + H = H_2 + F$		−9.44	0.00	17000	19
(17)	$I + I + M = I_2 + M$		−34.57	1.00	0	19
(18)	$I + H + M = HI + M$		−34.48	1.00	0	19
(19)	$I_2 + H = HI + I$		−9.39	0.00	0	19
(20)	$HI + H = H_2 + I$		−10.26	0.00	0	19
(21)	$Cl + Cl + M = Cl_2 + M$		−33.26	0.00	−900	19
(22)	$Cl + H + M = HCl + M$		−38.78	1.00	−18400	19
(23)	$Cl_2 + H = HCl + Cl$		−9.21	0.00	910	19
(24)	$HCl + H = H_2 + Cl$		−16.07	1.72	1010	20
(25)	$H + H + M = H_2 + M$		−29.56	−1.00	0	13

[a] Forward rate coefficients in the form $k = AT^n \exp(-E_a/RT)$, in cm^3, molecule, and s units. Reverse rate coefficients were calculated from the forward ones and the equilibrium constants.

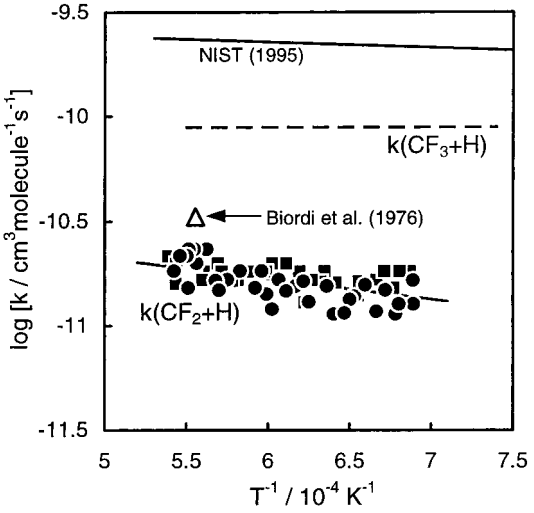

Figure 4. Arrhenius plot of the rate coefficients for the $CF_2(X^1A_1)$ + H reaction. (●) and (■) denote the present results measured at [M] = 6.2×10^{18} and 1.2×10^{19} molecules cm^{-3}, respectively. (△) denotes the previous value reported by Biordi et al.[11] Solid line (—) denotes the recommended data by the NIST group.[1] (- - -) denotes the rate coefficient for the CF_3 + H reaction determined by our group.[4]

$$k_2 = 10^{-10.18\pm0.21} \exp[-(19.0 \pm 6.7)\ \text{kJ mol}^{-1}/RT]$$
$$\text{cm}^3\ \text{molecule}^{-1}\ \text{s}^{-1}$$

where the error limits are given at the two standard deviation level.

Discussion

In the present study, although the test-gas mixtures highly diluted in argon were used to avoid the influence of secondary reactions, sensitivity analyses for each reaction listed in Tables 2 and 4 were still made by using the CHEMKIN-II[21] and SENKIN[22] program codes. In $CHClF_2-N_2O-Ar$ mixtures, a typical time-resolved profile of the normalized first-order sensitivity coefficient for O atom concentration, $\partial(\log[O])/(\partial \log k_j)$, is shown in Figure 5. The analysis shows that other

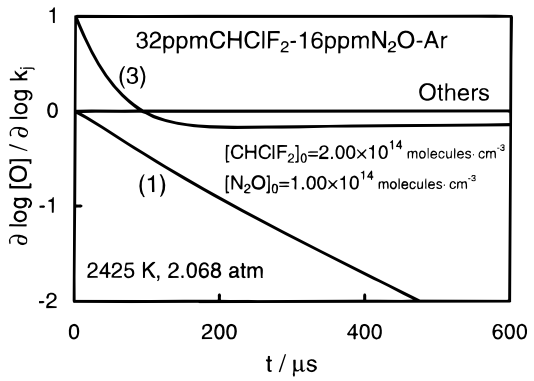

Figure 5. Sensitivity analysis of the rate coefficients for O atom concentration in 32 ppm of $CHClF_2$−16 ppm of N_2O−Ar mixture. Numbers in the figure denote the reaction numbers given in Table 2.

side reactions besides reactions 1 and 3, including reaction 6 after the focus reaction 1, have no influence on O atom concentration. Reaction 3 is the most sensitive until 70 μs when the O atom concentration gets to a maximum (cf. Figure 1b), but the focus reaction 1 more strongly affects the O atom concentration, rather than reaction 3, after 70 μs. The kinetic data for reaction 3 have already been reported by numerous workers. Some extensive literature reviews[23−25] about it also have been published. If this k_3 has a large error, the calculated O atom concentration profiles cannot be fitted to the observed ones by adjusting k_1 only, because reaction 3 has more sensitivity at the early stage of reaction time but reaction 1 contributes later. So, the uncertainty of k_3 cannot be considered to influence the determination of k_1 directly, and the present experimental results of k_1 can be concluded to have high accuracy.

Figure 6 shows a typical example of the results of sensitivity analysis in $CHClF_2-C_2H_5I-Ar$ mixtures. Reaction 2 is the most sensitive for H atom concentration, indicating that the present experimental conditions are appropriate to derive k_2. In contrast, the concentration of H atoms are never affected by reactions 4, 7, 10−23, and 25. Reactions 9a and 9b are the thermal decomposition of C_2H_5I, which is related to the formation of H

TABLE 5: Summary of Rate Coefficients Measured for the Reaction $CF_2(X^1A_1) + H \rightarrow CF + HF$

		reflected shock region				
P_1[a] Torr	U_s[b] m ms^{-1}	T K	[M] molecules cm^{-3}	[$CHClF_2$]$_0$ molecules cm^{-3}	[C_2H_5I]$_0$ molecules cm^{-3}	k_2 cm^3 molecule^{-1} s^{-1}
			[M] = 6.1×10^{18} molecules cm^{-3}			
35.0	0.780	1451	6.20×10^{18}	9.92×10^{13}	1.24×10^{13}	1.26×10^{-11}
35.0	0.780	1452	6.20×10^{18}	9.92×10^{13}	1.24×10^{13}	1.64×10^{-11}
35.0	0.785	1470	6.24×10^{18}	9.99×10^{13}	1.25×10^{13}	1.26×10^{-11}
35.0	0.787	1475	6.25×10^{18}	1.00×10^{14}	1.25×10^{13}	1.13×10^{-11}
35.0	0.791	1488	6.29×10^{18}	1.01×10^{14}	1.26×10^{13}	1.48×10^{-11}
34.0	0.794	1501	6.13×10^{18}	9.82×10^{13}	1.23×10^{13}	1.16×10^{-11}
34.0	0.799	1516	6.17×10^{18}	9.87×10^{13}	1.23×10^{13}	1.56×10^{-11}
34.0	0.803	1532	6.20×10^{18}	9.92×10^{13}	1.24×10^{13}	1.38×10^{-11}
34.0	0.805	1538	6.21×10^{18}	9.95×10^{13}	1.24×10^{13}	1.33×10^{-11}
34.0	0.807	1546	6.23×10^{18}	9.97×10^{13}	1.25×10^{13}	1.15×10^{-11}
34.0	0.812	1562	6.27×10^{18}	1.00×10^{14}	1.25×10^{13}	1.13×10^{-11}
33.0	0.815	1572	6.11×10^{18}	9.77×10^{13}	1.22×10^{13}	1.54×10^{-11}
33.0	0.822	1600	6.16×10^{18}	9.86×10^{13}	1.23×10^{13}	1.30×10^{-11}
33.0	0.825	1609	6.18×10^{18}	9.89×10^{13}	1.24×10^{13}	1.63×10^{-11}
33.0	0.828	1621	6.20×10^{18}	9.92×10^{13}	1.24×10^{13}	1.54×10^{-11}
33.0	0.833	1636	6.23×10^{18}	9.97×10^{13}	1.25×10^{13}	1.46×10^{-11}
33.0	0.836	1649	6.26×10^{18}	1.00×10^{14}	1.25×10^{13}	1.66×10^{-11}
33.0	0.839	1660	6.28×10^{18}	1.00×10^{14}	1.26×10^{13}	1.20×10^{-11}
32.0	0.842	1669	6.11×10^{18}	9.77×10^{13}	1.22×10^{13}	1.41×10^{-11}
32.0	0.844	1677	6.12×10^{18}	9.79×10^{13}	1.22×10^{13}	1.83×10^{-11}
32.0	0.847	1689	6.14×10^{18}	9.83×10^{13}	1.23×10^{13}	1.51×10^{-11}
32.0	0.854	1716	6.19×10^{18}	9.90×10^{13}	1.24×10^{13}	1.83×10^{-11}
32.0	0.860	1739	6.23×10^{18}	9.97×10^{13}	1.25×10^{13}	1.66×10^{-11}
32.0	0.865	1755	6.26×10^{18}	1.00×10^{14}	1.25×10^{13}	1.48×10^{-11}
32.0	0.866	1760	6.26×10^{18}	1.00×10^{14}	1.25×10^{13}	1.61×10^{-11}
32.0	0.866	1761	6.27×10^{18}	1.00×10^{14}	1.25×10^{13}	1.64×10^{-11}
32.0	0.871	1778	6.29×10^{18}	1.01×10^{14}	1.26×10^{13}	2.32×10^{-11}
32.0	0.876	1798	6.33×10^{18}	1.01×10^{14}	1.27×10^{13}	1.99×10^{-11}
32.0	0.877	1803	6.34×10^{18}	1.01×10^{14}	1.27×10^{13}	2.32×10^{-11}
32.0	0.880	1813	6.35×10^{18}	1.02×10^{14}	1.27×10^{13}	2.32×10^{-11}
31.0	0.880	1815	6.15×10^{18}	9.85×10^{13}	1.23×10^{13}	1.51×10^{-11}
31.0	0.881	1817	6.16×10^{18}	9.86×10^{13}	1.23×10^{13}	2.16×10^{-11}
31.0	0.885	1831	$6.^{18} \times 10^{18}$	9.89×10^{13}	1.24×10^{13}	2.16×10^{-11}
32.0	0.888	1843	6.40×10^{18}	1.02×10^{14}	1.28×10^{13}	1.83×10^{-11}
			[M] = 1.2×10^{19} molecules cm^{-3}			
69.0	0.781	1456	1.22×10^{19}	9.79×10^{13}	1.22×10^{13}	1.83×10^{-11}
69.0	0.785	1470	1.23×10^{19}	9.84×10^{13}	1.23×10^{13}	1.83×10^{-11}
68.0	0.788	1478	1.22×10^{19}	9.73×10^{13}	1.22×10^{13}	1.51×10^{-11}
68.0	0.791	1490	1.22×10^{19}	9.77×10^{13}	1.22×10^{13}	1.83×10^{-11}
68.0	0.794	1501	1.23×10^{19}	9.81×10^{13}	1.23×10^{13}	1.66×10^{-11}
67.0	0.801	1525	1.22×10^{19}	9.76×10^{13}	1.22×10^{13}	1.63×10^{-11}
67.0	0.802	1527	1.22×10^{19}	9.76×10^{13}	1.22×10^{13}	1.39×10^{-11}
67.0	0.803	1530	1.22×10^{19}	9.77×10^{13}	1.22×10^{13}	1.38×10^{-11}
66.0	0.811	1559	1.22×10^{19}	9.73×10^{13}	1.22×10^{13}	1.61×10^{-11}
66.0	0.816	1576	1.22×10^{19}	9.78×10^{13}	1.22×10^{13}	1.83×10^{-11}
65.0	0.817	1582	1.21×10^{19}	9.65×10^{13}	1.21×10^{13}	1.63×10^{-11}
65.0	0.821	1596	1.21×10^{19}	9.70×10^{13}	1.21×10^{13}	1.66×10^{-11}
65.0	0.824	1607	1.22×10^{19}	9.73×10^{13}	1.22×10^{13}	1.30×10^{-11}
65.0	0.827	1616	1.22×10^{19}	9.76×10^{13}	1.22×10^{13}	1.83×10^{-11}
65.0	0.833	1637	1.23×10^{19}	9.82×10^{13}	1.23×10^{13}	1.99×10^{-11}
64.0	0.839	1660	1.22×10^{19}	9.74×10^{13}	1.22×10^{13}	1.99×10^{-11}
64.0	0.842	1670	1.22×10^{19}	9.77×10^{13}	1.22×10^{13}	1.83×10^{-11}
63.0	0.850	1700	1.21×10^{19}	9.70×10^{13}	1.21×10^{13}	1.83×10^{-11}
63.0	0.855	1720	1.22×10^{19}	9.76×10^{13}	1.22×10^{13}	1.66×10^{-11}
63.0	0.858	1731	1.22×10^{19}	9.79×10^{13}	1.22×10^{13}	1.64×10^{-11}
63.0	0.863	1750	1.23×10^{19}	9.84×10^{13}	1.23×10^{13}	1.83×10^{-11}
63.0	0.865	1757	1.23×10^{19}	9.86×10^{13}	1.23×10^{13}	1.99×10^{-11}
62.0	0.868	1766	1.22×10^{19}	9.73×10^{13}	1.22×10^{13}	1.83×10^{-11}
62.0	0.872	1784	1.22×10^{19}	9.77×10^{13}	1.22×10^{13}	1.83×10^{-11}
62.0	0.873	1787	1.22×10^{19}	9.78×10^{13}	1.22×10^{13}	1.66×10^{-11}
62.0	0.877	1802	1.23×10^{19}	9.82×10^{13}	1.23×10^{13}	1.99×10^{-11}
61.0	0.885	1834	1.22×10^{19}	9.74×10^{13}	1.22×10^{13}	1.99×10^{-11}
61.0	0.887	1839	1.22×10^{19}	9.75×10^{13}	1.22×10^{13}	1.99×10^{-11}
61.0	0.887	1840	1.22×10^{19}	9.76×10^{13}	1.22×10^{13}	1.59×10^{-11}
61.0	0.891	1856	1.22×10^{19}	9.79×10^{13}	1.22×10^{13}	2.16×10^{-11}

[a] Pressure ahead of incident shock wave. [b] Incident shock velocity.

atoms. The kinetic data for reactions 9a and 9b cited in the present work have been directly and exactly measured by using a shock tube/ARAS technique by our group. Kumaran et al.[26] have also determined them experimentally to be k_{9a} =

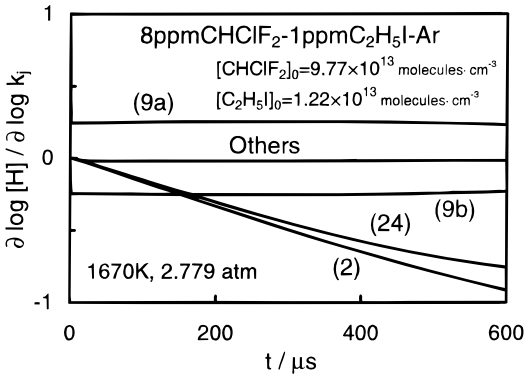

Figure 6. Sensitivity analysis of the rate coefficients for H atom concentration in 8 ppm of $CHClF_2$−1 ppm of C_2H_5I−Ar mixture. Numbers in the figure denote the reaction numbers given in Table 4.

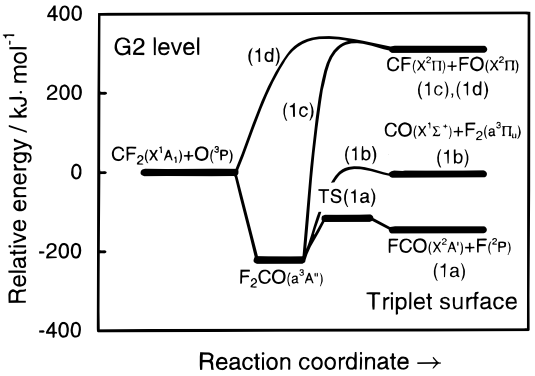

Figure 7. Energy diagram on the triplet surface for the $CF_2(X^1A_1)$ + O reaction. The energies are calculated at the G2 level and are corrected for the zero-point vibrations.

$10^{9.80}$ exp(−132 kJ mol^{-1}/RT) cm^3 molecule^{-1} s^{-1} with an error limit of ±76% and $k_{9a}/(k_{9a} + k_{9b}) = 0.85 \pm 0.07$. The values of k_2 determined by using their k_{9a} and k_{9b} agreed with the results summarized in Table 5 within the limits of experimental errors. Therefore, these rate coefficients cannot create a large error in the determination of k_2. Reaction 24 is the most sensitive to H atom concentration after reaction 2, because hydrogen chloride is the other product formed by the thermal decomposition of $CHClF_2$. So, the kinetic data for reaction 24 have to be selected carefully. Although the experimental data of k_{24} had previously been reported by numerous workers,[27−32] most of them were measured at relatively low temperatures below 1200 K. Among these data, the maximum value[28] is 5 times larger than the minimum one.[29] This difference of k_{24} causes an error of 50% for k_2. In the present computation, the value of k_{24} was taken from the kinetic data for the reverse reaction $H_2 + Cl \rightarrow HCl + H$, which were published by Kumaran et al.[20] Their rate coefficient is the most reliable in the previous data, because it has precisely been measured over the extremely wide temperature range 296−3000 K by using three modern experimental techniques. Therefore, the present experimental results of k_2 are estimated to contain an error of only ±5%, due to the uncertainty of ±17% for k_{24}.

To examine the product channels for the $CF_2(X^1A_1) + O(^3P)$ and $CF_2(X^1A_1)$ + H reactions, ab initio MO calculations were performed by using the Gaussian 94 program.[33] Figure 7 shows the energy diagram on the triplet surface for the $CF_2(X^1A_1)$ + O reaction calculated at the G2 level. In this system, two kinds of processes are possible: decompositions following an electrophilic addition of $O(^3P)$ to $CF_2(X^1A_1)$ radical (channels 1a−c) and abstraction of F atom by the $O(^3P)$ (channel (1d)). Since the addition step of $O(^3P)$ atom is greatly exothermic, a

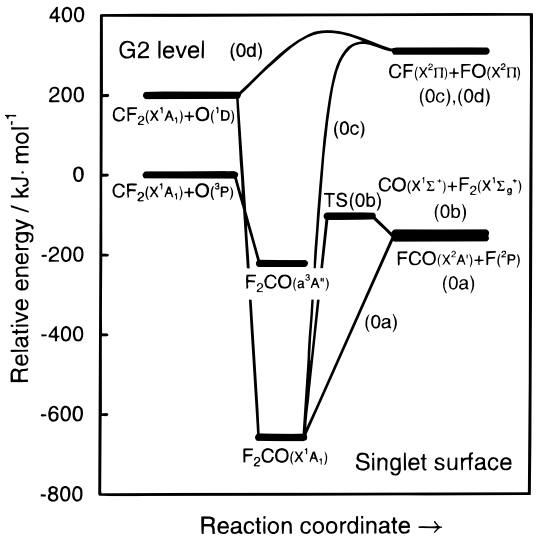

Figure 8. Energy diagram on the singlet surface for the $CF_2(X^1A_1)$ + O reaction. The energies are calculated at the G2 level and are corrected for the zero-point vibrations.

chemically activated energized triplet-state intermediate, $F_2CO^*(a^3A'')$, is formed. Subsequently, $F_2CO^*(a^3A'')$ is decomposed through the steps of F dissociation (1a), F_2 elimination (1b), or FO elimination (1c). The energy of the transition state for channel (1a) is much lower than the energies of products for other channels including the abstraction one, as shown in Figure 7. Therefore, we can conclude that the most energetically favorable pathway on the triplet surface for the $CF_2(X^1A_1)$ + O system is the formation of $F_2CO^*(a^3A'')$ by the addition of $O(^3P)$ to $CF_2(X^1A_1)$ radical and then the dissociation to FCO and F. The formation of the most stable singlet state intermediate $F_2CO^*(X^1A_1)$ from $CF_2(X^1A_1) + O(^3P)$ is a spin-forbidden process. However, the spin conservation is not a strict rule if the triplet surface can cross the singlet one in this system. Figure 8 shows the singlet potential energy diagram for the $CF_2(X^1A_1)$ + O reaction. Two product channels of F dissociation (0a) and F_2 elimination (0b) are exothermic on the singlet surface. Although the energies of products are almost same between channels 0a and 0b, the energy of the transition state for channel 0b is 55 kJ mol^{-1} higher, leading the dominance of channel 0a. Therefore, it is needless to alter our conclusion that the main products for the $CF_2(X^1A_1) + O(^3P)$ reaction are FCO and F, even if the crossing from the triplet surface to the singlet one occurs.

The energy diagram for the $CF_2(X^1A_1)$ + H reaction is shown in Figure 9. Similarly to the $CF_2(X^1A_1) + O(^3P)$ system, possible channels are decompositions of the activated adduct CHF_2^* (channels 2a−c) and abstraction of F (channel 2d). Vibrationally excited CHF_2^*, which is formed by an addition of H to $CF_2(X^1A_1)$ radical, is decomposed through the steps of F dissociation (2a), F_2 elimination (2b), or HF elimination (2c). In the three channels for the CHF_2^* decomposition, channel 2c is the most energetically favorable, as shown in Figure 9. Although abstraction channel 2d produces the same species as channel 2c, the energy of the transition state for channel 2d is higher by 148 kJ mol^{-1} than that for channel 2c. So, the reaction pathway for the $CF_2(X^1A_1)$ + H system can be concluded to be the formation of CF and HF through the three-centered HF elimination channel (2c), but not through the abstraction channel (2d).

In the present experimental results, we found a difference between the two rate coefficients; k_1 has no temperature dependence, but k_2 has a little temperature dependence, although

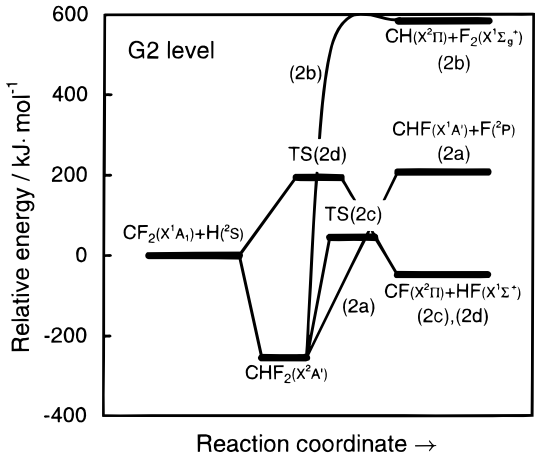

Figure 9. Energy diagram for the $CF_2(X^1A_1)$ + H reaction. The energies are calculated at the G2 level and are corrected for the zero-point vibrations.

both were the rate coefficients for atom−radical reactions. As shown in Figures 7−9, the most energetically favorable channel (1a) has no barrier throughout the reaction path in the $CF_2(X^1A_1)$ + $O(^3P)$ system, while the energy of the transition state for channel 2c is 45 kJ mol^{-1} higher than that of the reactants $CF_2(X^1A_1)$ + H. These theoretical results can qualitatively explain the temperature dependence of the experimentally determined rate coefficients.

Several previous high-temperature kinetic data for the $CF_2(X^1A_1)$ + $O(^3P)$ and $CF_2(X^1A_1)$ + H reactions are shown in Figures 2 and 4, respectively, compared to the present experimental results. At 1800 K, the kinetic data reported by Biordi et al.[11] are 2.0 times larger for the $CF_2(X^1A_1)$ + $O(^3P)$ reaction and 1.8 times larger for the $CF_2(^1A_1)$ + H reaction than the present results. However, there is some possibility that their experimental values have significant errors, because they were determined in methane−oxygen−argon flames containing CF_3Br where complicated branching reactions occur simultaneously. Hence, the disagreements between Biordi et al. and the present work may not be significant. The high-temperature rate coefficients published in the NIST kinetic model are simply estimated values obtained by giving small activation barriers to the room-temperature values of Tsai and McFadden.[6,10] However, no reasons are given as to why the values of 4−5 kJ mol^{-1} were applied to the activation barriers for these reactions. For the $CF_2(X^1A_1)$ + $O(^3P)$ reaction, although the rate coefficient evaluated by the NIST group is 2.2−2.3 times lager than the present experimental results over the temperature range 2000−2430 K, this disagreement can be solved by reducing their activation energy of 4.2 kJ mol^{-1} to 1.6 kJ mol^{-1}. This minor revision for the NIST evaluation is acceptable. On the other hand, for the $CF_2(X^1A_1)$ + H reaction, the rate coefficient estimated by the NIST group is 12−16 times larger than the present data over the temperature range 1450−1860 K. The NIST group cites the room-temperature value of Tsai and McFadden[10] as a reference point. As mentioned above, however, the $k(CF_2+H)$ values are still unsettled even at room temperature. Ryan and Plumb[9] first measured the room-temperature data for $k(CF_2+H)$ and reported to be $(1.7 \pm 0.4) \times 10^{-13}$ cm^3 molecule^{-1} s^{-1}, which is much smaller than that of Tsai and McFadden. When the present result for $k(CF_2+H)$ is extrapolated to lower temperatures, our estimated value at room temperature agrees with the data of Ryan and Plumb at the 95% confidence level. This fact means that the data of Ryan and Plumb is more reasonable at room temperature than those of Tsai and McFadden.

The rate coefficients determined in the present work show that $CF_2(X^1A_1)$ radicals could react with $O(^3P)$ atoms more easily than with H atoms, differing from CF_3 radicals of which the reactivity was discussed previously.[4] As shown with the broken lines in Figures 2 and 4, the relations of rate coefficients between the reactions of $CF_2(X^1A_1)$ and CF_3 radicals can be expressed as $k(CF_2+O) > k(CF_3+O)$ and $k(CF_2+H) < k(CF_3+H)$. The following reasons can explain those relations. The reaction pathway for the $CF_2(X^1A_1)$ + $O(^3P)$ system are very similar to that for the CF_3 + $O(^3P)$ system; the addition steps of $O(^3P)$ atom to these radicals occur initially, and then the activated energized adducts, F_2CO^* and F_3CO^*, are dissociated to FCO + F and F_2CO + F. As both reaction pathways have no energy barrier, the relative reactivity might depend on their electronic degeneracies. The ratio of electronic partition functions between the $CF_2(X^1A_1)$ + $O(^3P)$ and CF_3 + $O(^3P)$ systems can be expressed as

$$\frac{Q_e(CF_2+O)}{Q_e(CF_3+O)} = \frac{g(F_2CO)/g(CF_2)}{g(F_3CO)/g(CF_3)}$$

where g's mean electronic degeneracies for species. The formula yields 1.5 for $Q_e(CF_2+O)/Q_e(CF_3+O)$,[34] which is nearly equal to the ratio of experimentally determined rate coefficients, $k(CF_2+O)/k(CF_3+O) = 1.6$. This agreement shows that the difference between $k(CF_2+O)$ and $k(CF_3+O)$ can be quantitatively explained only by their electronic degeneracies. Also for $CF_2(X^1A_1)$ + H and CF_3 + H reactions, reaction pathways are similar to each other: the three-centered eliminations of HF occur via the activated energized adducts CHF_2^* and CHF_3^*. Although the energy gap between the adduct and the three-centered transition state for the $CF_2(X^1A_1)$ + H system is almost the same as that for the CF_3 + H system, the stabilization energy from the reactant to the adduct for the $CF_2(X^1A_1)$ + H system is 191 kJ mol^{-1} smaller than that for the CF_3 + H system. This difference in the relative stabilities of the adducts causes the process producing $CF_2(X^1A_1)$ + HF from CF_3 + H to have no barrier throughout the reaction path and the process producing CF + HF from $CF_2(X^1A_1)$ + H to have a small barrier, leading to the relation $k(CF_2+H) < k(CF_3+H)$.

Conclusions

This study on kinetics of the high-temperature reactions of $CF_2(X^1A_1)$ with $O(^3P)$ and H atoms can be summarized as follows.

(a) The $CF_2(X^1A_1)$ + $O(^3P)$ and $CF_2(X^1A_1)$ + H reactions proceed through F dissociation and HF elimination following their electrophilic additions.

(b) The rate coefficients for the reactions $CF_2(X^1A_1)$ + $O(^3P) \rightarrow$ FCO + F (1) and $CF_2(X^1A_1)$ + H → CF + HF (2) were experimentally determined to be $k_1 = 10^{-10.39\pm0.07}$ and $k_2 = 10^{-10.18\pm0.21} \exp[-(19.0 \pm 6.7)\text{ kJ mol}^{-1}/RT]$ cm^3 molecule^{-1} s^{-1} over the temperature ranges 2000−2430 and 1450−1860 K, respectively. This difference in temperature dependence between k_1 and k_2 could also be supported by the G2-level ab initio MO calculation.

(c) From comparison of the rate coefficients, the dominant channel of $CF_2(X^1A_1)$ consumption in the combustion is estimated to be the reaction with $O(^3P)$ atoms, but not H atoms, differing from CF_3 consumption.

Acknowledgment. The authors express gratitude to Professor Frank Scott Howell S. J. for his valuable comments.

References and Notes

(1) Burgess, D. R. F., Jr.; Zachariah, M.; Tsang, W.; Westmoreland, P. R. *Prog. Energy Combust. Sci.* **1995**, *21*, 453.

(2) Sanogo, O.; Delfau, J.-L.; Akrich, R.; Vovelle, C. *Prog. Combust. Sci. Technol.* **1997**, *122*, 33.

(3) Takahashi, K.; Yamamori, Y.; Inomata, T. *J. Phys. Chem. A* **1997**, *101*, 9105.

(4) Takahashi, K.; Sekiuji, Y.; Yamamori, Y.; Inomata, T. *J. Phys. Chem. A* **1998**, *102*, 8339.

(5) Ryan, K. R.; Plumb, I. C. *Plasma Chem. Plasma Proc.* **1984**, *4*, 271.

(6) Tsai, C.; McFadden, D. L. *Chem. Phys. Lett.* **1990**, *173*, 241.

(7) Hancock, G.; Harrison, P. D.; MacRobert, A. J. *J. Chem. Soc., Faraday Trans. 2* **1986**, *82*, 647.

(8) Yamazaki, K.; Tanaka, A.; Watanabe, A.; Yokoyama, K.; Tokue, I. *J. Phys. Chem.* **1995**, *99*, 15086.

(9) Ryan, K. R.; Plumb, I. C. *Plasma Chem. Plasma Proc.* **1984**, *4*, 141.

(10) Tsai, C.; McFadden, D. L. *J. Phys. Chem.* **1989**, *93*, 2471.

(11) Biordi, J. C.; Lazzara, C. P.; Papp, J. F. *J. Phys. Chem.* **1976**, *80*, 1042.

(12) Su, M.-C.; Kumaran, S. S.; Lim, K. P.; Michael, J. V.; Wagner, A. F. *J. Phys. Chem.* **1996**, *100*, 15827.

(13) Miller, J. A.; Bowman, C. T. *Prog. Energy Combust. Sci.* **1989**, *15*, 287.

(14) Westbrook, C. K. *Combust. Sci. Technol.* **1983**, *34*, 201.

(15) Tyerman, W. J. R. *J. Chem. Soc., Faraday Trans.* **1969**, *65*, 1188.

(16) Baulch, D. L.; Drysdale, D. D.; Duxbury, J.; Grant, S. J. *Evaluated Kinetic Data for High-Temperature Reactions. Volume 3 Homogeneous Gas-Phase Reactions of the O_2-O_3 System, the $CO-O_2$-H_2 System, and of Sulphur-containing Species*; Butterworth: London, 1976; p 33.

(17) Richter, H.; Vandooren, J.; Van Tiggelen, P. J. *J. Chim. Phys.* **1994**, *91*, 1748.

(18) Okada, K. Master Thesis, Sophia University, 1996.

(19) Westbrook, C. K. *Nineteenth Symposium (International) on Combustion*; The Combustion Institute: Pittsburgh, PA, 1982; p 127.

(20) Kumaran, S. S.; Lim, K. P.; Michael, J. V. *J. Chem. Phys.* **1994**, *101*, 9487.

(21) Kee, R. J.; Rupley, F. M.; Miller, J. A. *Chemkin- II: A Fortran Chemical Kinetics Package for the Analysis of Gas-Phase Chemical Kinetics*; Sandia National Laboratories Report SAND89-8009; Sandia Laboratories: Albuquerque, NM, 1993.

(22) Lutz, A. E.; Kee, R. J.; Miller, J. A. *SENKIN: A Fortran Program for Predicting Homogeneous Gas-Phase Chemical Kinetics with Sensitivity Analysis*; Sandia National Laboratories Report SAND87-8248; Sandia Laboratories: Albuquerque, NM, 1991.

(23) Hanson, R. K.; Salimian, S. In *Combustion Chemistry*; Gardiner, W. C., Jr., Ed.; Springer-Verlag: New York, 1984; p 361.

(24) Tsang, W.; Herron, J. T. *J. Phys. Chem. Ref. Data* **1991**, *20*, 609.

(25) Ross, S. K.; Sutherland, J. W.; Kuo, S.-C.; Klemm, R. B. *J. Phys. Chem. A* **1997**, *101*, 1104.

(26) Kumaran, S. S.; Su, M.-C.; Lim, K. P.; Michael, J. V. *Twenty-sixth Symposium (International) on Combustion*; The Combustion Institute: Pittsburgh, PA, 1996; p 605.

(27) Clyne, M. A. A.; Stedman, D. H. *Trans. Faraday Soc.* **1966**, *62*, 2164.

(28) Westenberg, A. A.; DeHaas, N. *J. Chem. Phys.* **1968**, *48*, 4405.

(29) Ambidge, P. F.; Bradley, J. N.; Whytock, D. A. *J. Chem. Soc., Faraday Trans. 1* **1976**, *72*, 2143.

(30) Miller, J. C.; Gordon, R. J. *J. Chem. Phys.* **1981**, *75*, 5305.

(31) Kita, D.; Stedman, D. H. *J. Chem. Soc., Faraday Trans. 2* **1982**, *78*, 1249.

(32) Adusei, G. Y.; Fontijn, A. *J. Phys. Chem.* **1993**, *97*, 1409.

(33) Frisch, M. J.; Trucks, G. W.; Schlegel, H. B.; Gill, P. M. W.; Johnson, B. G.; Robb, M. A.; Cheeseman, J. R.; Keith, T.; Petersson, G. A.; Montgomery, J. A.; Raghavachari, K.; Al-Laham, M. A.; Zakrzewski, V. G.; Ortiz, J. V.; Foresman, J. B.; Cioslowski, J.; Stefanov, B. B.; Nanayakkara, A.; Challacombe, M.; Peng, C. Y.; Ayala, P. Y.; Chen, W.; Wong, M. W.; Andres, J. L.; Replogle, E. S.; Gomperts, R.; Martin, R. L.; Fox, D. J.; Binkley, J. S.; Defrees, D. J.; Baker, J.; Stewart, J. P.; Head-Gordon, M.; Gonzalez, C.; Pople, J. A. *Gaussian 94W*, revision D.3; Gaussian, Inc.: Pittsburgh, PA, 1995.

(34) Note $g(F_3CO) = 4$ because the Jahn−Teller distortion from the 2E state for F_3CO is small and the resulting 2A′ and 2A″ states are nearly degenerate with a splitting energy of less than 1 kJ mol^{-1}.